Magnetism in High-Resolution NMR Probe Design. I: General Methods

F. DAVID DOTY,* GEORGE ENTZMINGER, Y. ANDY YANG

Doty Scientific, Inc., 700 Clemson Rd., Columbia, SC 29229; Phone: 803-788-6497; Fax: 803-736-5495; E-mail: david@doty.usa.com

ABSTRACT: In Part I, we review some basic physics, properties, and types of magnetism as they relate to high-resolution nuclear magnetic resonance (NMR) probe design, both in liquids and in solids, and some of the reasons it is technically difficult to obtain resolution of several parts per billion. We note the beneficial attributes of elliptical symmetries and the finite magic angle cylinder; and some methods of calculating fields produced by various objects are reviewed, with emphasis on the method of effective surface currents. Using a novel dual-ring method, the high-field magnetic properties of various materials important to NMR probe construction are obtained. Methods of adjusting and controlling the susceptibility of special adhesives, wire, foil, and dewar alloys are discussed. In Part II, we will look more specifically at high-resolution magic angle spinning probe design issues. Concepts Magn Reson 10: 133–156, 1998

KEY WORDS: magnetism; susceptibility; probes; MAS; coils; alloys; resolution; dielectrics

INTRODUCTION

The importance of high resolution (HR) nuclear magnetic resonance (NMR) for resolving closely spaced lines in relatively simple molecules was apparent within a few years after initial NMR experiments in the late forties, and Varian and Bruker both achieved a resolution of 0.5 Hz at 60 MHz by the late fifties. However, the impact of resolution on signal-to-noise (S/N) was fully appreciated only after the development of Fourier transform (FT) NMR by Ernst in the midsixties, as the FT method made it possible to obtain the S/N benefit of a very narrow effective noise bandwidth without limiting the spectral bandwidth. However, as improved sensitivity made it possible to extend NMR to dilute samples, it became clear that resolution alone [defined as the linewidth at 50% height; also called full width half height (FWHH or FWHM)] was not sufficient. Line shape was just as important. That is, the linewidth at 10%, 1%, and 0.1% of full height must be very close to the ideal Lorentzian line shape for most solvent suppression techniques to be effective and to allow low-level constituents near a large solvent signal to be resolved, although it is possible that spectral data processing based on recent advances in information theory

Received October 31, 1997; revised January 6, 1998; accepted January 8, 1998.

*To whom correspondence should be addressed.

Concepts in Magnetic Resonance, Vol. 10(3) 133–156 (1998)
 CCC 1043-7347/98/030133-24

and wavelet theory could make line shape less critical in the next decade.

Modern HR NMR spectrometers achieve linewidth approaching 1 part per billion (ppb) with nearly ideal line shape on liquids without sample spinning, and some of the latest NMR probes for solid samples come within a factor of two of this amazing achievement under magic angle spinning (MAS). To the casual user, it may not be immediately obvious that such resolution is truly amazing, but consider this. Place a small piece of just about any nonmagnetic material (such as pure copper or quartz, for example) near the sample, and resolution is likely to be degraded by about two orders of magnitude because of the material's magnetization. Moreover, shimming is not likely to be very effective in correcting the problem.

Yet, no area of critical importance to NMR technology has been more shrouded in mystery or more ignored in the professional literature than the technical issues related to achieving HR. More than 20 years ago, Hoult addressed some of the basic issues in his classic overview of NMR spectrometer design (*1*), and a few publications, patents, and presentations during the ensuing 15 years provided some clues into the technology; but for the most part it was kept cloaked in secrecy, even though at least 40 papers and an equal number of patents appeared during this period dealing with probe-related issues [mostly radiofrequency (rf) and sample-handling technology]. The reason for the dearth of technical detail was the intense industrial competition. (Even though today there is no significant difference between the state of this technology among the major NMR vendors, at least one NMR spectrometer manufacturer still keeps its HR technology under such strict control that only a handful of its scientists and engineers are even permitted into the areas of the building where HR probes are assembled or repaired.) Obviously, we, too, are in a competitive industrial setting and are forced to be concerned about intellectual property, but we have generally opted to take the patenting route rather than the confidential route. Fortunately, several papers finally came out of industry on some aspects of magnetism in HR probe design in recent years (*2*, *3*). This two-part series should help to fill in many of the missing pieces in the puzzle.

While our main interest has always been in solids probes (*4*, *5*), it was becoming clear by early 1993 that there would be many semisolids applications demanding resolution comparable to what had previously been thought possible only with liquids. At the same time, it was also becoming clear that ultra-high-field liquids probes needed to borrow some of the high-power technology developed by the solids probe builders—mainly because the chemical shift scales with B_0, thus requiring ever shorter $\pi/2$ pulses. Hence, the distinction between liquids and solids NMR probe technology has become a little blurred. The case study at the end of Part II will return our focus to magnetic issues related to HR MAS of solids and semisolids, as we look more closely at a particular design that is compatible with variable angle spinning (VAS), sample eject, and high-power decoupling of biological samples at the highest fields.

MAGNETISM: BASIC CONCEPTS

Prior to some recent demonstrations of new bulk magnetic susceptibility (BMS) effects in liquids, NMR spectroscopists have generally focused exclusively on atomic-level, molecular-level, and free-space electromagnetic interactions. (The probable reason for a general lack of interest in BMS effects is that researchers soon learned that the dissolution of an inert internal reference compound in a physically homogeneous solution effectively eliminated the BMS shift, but we will show susceptibility is critical in probe design.) Since there has seldom been any reason to worry about magnetic field strength (or intensity) **H** (A/m) in NMR, the term "magnetic field" has been applied commonly to the magnetic flux density **B** (W/m^2).

The basic relationships in SI units between the fields, magnetization **M** (dipole moment per unit volume), (dimensionless) susceptibility χ, and relative (dimensionless) permeability μ, are:

$$\mathbf{M} = \chi\mathbf{H} \qquad [1]$$

$$\mu = 1 + \chi \qquad [2]$$

$$\mathbf{B} = \mu_0(\mathbf{H} + \mathbf{M}) = \mu\mu_0\mathbf{H} \qquad [3]$$

$$M = \frac{\chi B_0}{\mu_0(1 + \chi)} \qquad [4]$$

Note that some authors (*2*) continue to use Gaussian or cgs units, which can be quite confusing, as even the dimensionless quantity χ differs by a factor of 4π, and μ_0 (the permeability of

free space, $4\pi \times 10^{-7}$ H/m) seems to come and go. Molar susceptibility χ_M in cgs units (which is more commonly published) is related to SI volumetric susceptibility by the following:

$$\chi = 4\pi d\chi_M/W \qquad [5]$$

where d is the density and W is the molecular weight.

Magnetization arises from lossless current loops within atoms, electrons, and nucleons in response to an external field. The total field when material is introduced into an external field is then the sum of the fields produced by external transport current and the atomic currents induced within the material.

Magnetization is a vector point function. Each macroscopic point represents the effects of a statistically large number of atomic current loops. Assume, for example, $\mathbf{H} = H_0\mathbf{e}_3$ (where $\mathbf{e}_3$ is the unit vector in the z direction). Then, each macroscopic volume element $\delta x\delta y\delta z$ may be represented by a single current loop I_z of area $\delta x\delta y$ as shown in Fig. 1. The magnetic moment δm_z of this element is

$$\delta m_z = M_z\,\delta x\delta y\delta z = I_z\,\delta x\delta y \qquad [6]$$

Note that for uniform magnetization, the currents everywhere within the material volume cancel, leaving only surface currents at the material boundaries. In the more general case, the magnetization need not be uniform, and it can be shown

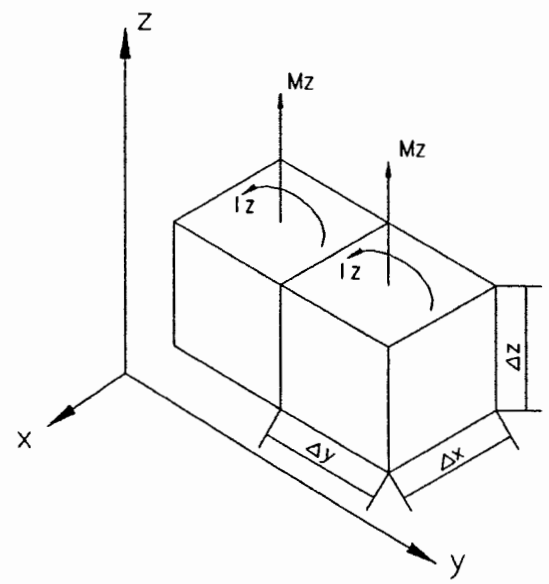

Figure 1 Macroscopic model of magnetism based on adjacent current loops.

than the magnetization current density $\mathbf{J}_M$ throughout the volume is given by $\mathbf{J}_M = \text{curl } \mathbf{M}$, but in practice, it is seldom necessary to deal with this situation.

Historically, it has often been useful in solving magnetization problems to cast them into the form of electrostatic problems with magnetic pole densities on opposite surfaces normal to the magnetization, as in the familiar bar magnet. This is still quite useful conceptually, as one may easily visualize all of the effects as conservative $1/r^2$ fields emanating from the poles, as with electric charges. The interested reader may refer to standard textbooks (*6*) or recent articles (*2*, *7*) for more detailed treatments, but there appears to be little need now for the formalism, as the calculations are more readily handled in software either by the surface currents or the dipole moment elements as discussed in the following section.

Calculating Fields Produced by Magnetic Materials

There are several convenient approaches to numerically modeling the magnetic susceptibility effects of materials. One approach is to divide the magnetic materials into finite volume elements, calculate the magnetic dipole moment of each element, then calculate the magnetic field at each point in space from each dipole and sum the fields.

The calculations may be simplified in the case of small χ—i.e., $\chi \ll 1$. Since M is typically four or five orders of magnitude smaller than H for all cases of interest in NMR, the local effects of M on H may be neglected in the calculation of M. Thus, M may be assumed to be independent of the geometry of the material or nearby materials.

$$M \cong \chi B_0/\mu_0 \qquad [7]$$

With the assumption that $\mathbf{B}_0$ is approximately constant, magnetic moments for each volume element are readily calculated using Eq. [6]. The distant field of a magnetic dipole $\mathbf{m}$ can be shown to be given by (*6*)

$$\mathbf{B}(\mathbf{r}) = \frac{\mu_0}{4\pi}\left(-\frac{\mathbf{m}}{r^3} + \frac{3(\mathbf{m}\cdot\mathbf{r})\mathbf{r}}{r^5}\right) \qquad [8]$$

Normally, in NMR probe design, $\mathbf{m} = m_z\mathbf{e}_3$, and only $B_z(\mathbf{r})$ is of interest, in which case

$$B_z(\mathbf{r}) = \frac{-\mu_0 m_z}{4\pi}\left(\frac{1 - 3\cos^2\theta}{r^3}\right) \qquad [9]$$

This approach may be preferable for calculations with highly irregular geometries, but it generally gives larger errors in the near-field (when r is not large compared to δx, δy, and δz), especially with irregular shapes.

Note that B_z vanishes in the far field on the surfaces of the magic angle cones ($\theta = \pm 54.7°$ with respect to the external field). That is, the magnetic field in the familiar dipolar field pattern of Fig. 2 is transverse everywhere on the surfaces of the magic angle conical surfaces. Although the transverse components of **B** are a maximum at the magic angle, this is immaterial in NMR because of the large external B_z. That is, a B_z perturbation of 10 ppm changes the magnitude of $\mathbf{B}_0$ by 10 ppm, but the vector addition of a B_x perturbation of 10 ppm to $\mathbf{B}_0$ changes the magnitude of $\mathbf{B}_0$ by only 0.05 ppb. We will return to this later in positioning magnetic perturbations.

An alternative approach to the calculation for materials of uniform magnetization is to replace the magnetic material with effective current distributions on the surfaces, as also given by Eq. [6]. This is fully equivalent, both inside and outside the material (*3*). The task then is to calculate the magnetic field throughout space from any known current distribution.

In 1820, just a few weeks after Oersted announced his discovery that currents produce magnetic effects, Ampere presented the results of a series of experiments which, when generalized and expressed in modern mathematical language, has come to be known as the Biot-Savart law. The field contribution $d\mathbf{B}(\mathbf{r}_f)$ for current element $I_i d\mathbf{l}_i$ at $\mathbf{r}_i$ is given by

$$d\mathbf{B}(\mathbf{r}_f) = \frac{\mu_0}{4\pi}\left(\frac{\mathbf{I}_i d\mathbf{l}_i \times (\mathbf{r}_f - \mathbf{r}_i)}{|\mathbf{r}_f - \mathbf{r}_i|^3}\right) \qquad [10]$$

The cyclic integral around each current path $\mathbf{l}_i$ is easily calculated analytically only in certain highly symmetric situations—examples include the field along the axis of a solenoid of any length, the field anywhere in space from an infinitely long straight wire, and the field outside an infinite solenoid. [The solutions may be found in any standard textbook on electricity and magnetism (*6*).] In fact, the primary motivation for the development of the concept of the magnetic vector potential **A** (where $\mathbf{B} = \text{curl } \mathbf{A}$) was to make

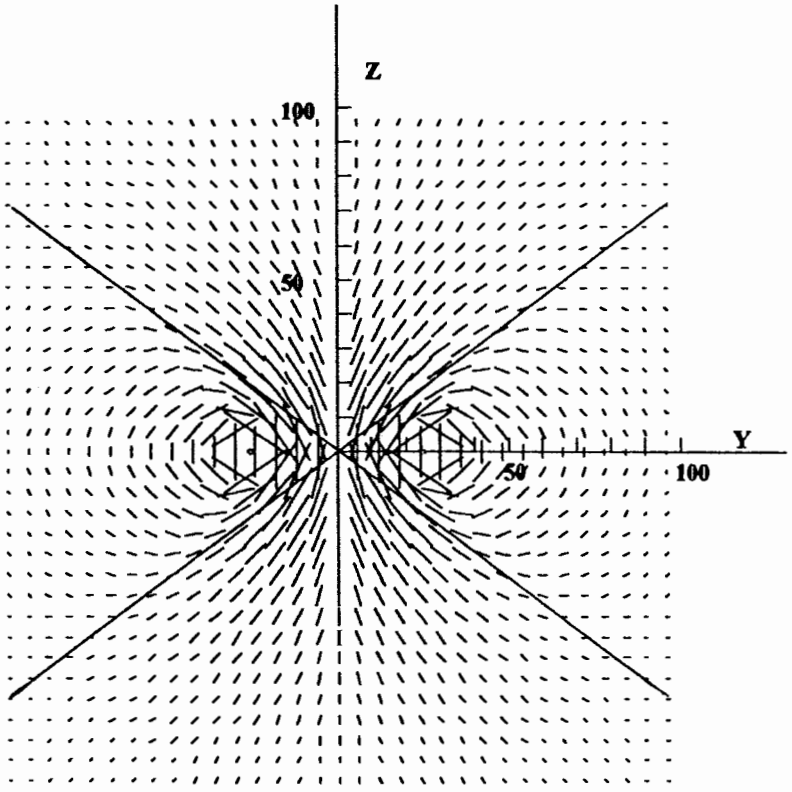

Figure 2 Dipolar field, represented by directed segments, from a current loop. Note that the z component vanishes at large distances along the magic angle.

it possible to solve a few more simple field problems—particularly, the far-field of a dipole, and some radiation problems. Obviously, the numerical integration of a single vector equation is straightforward with a computer. It is simply a matter of developing convenient and efficient software, as a typical problem may require defining thousands of current loops and performing 10^7 to 10^9 matrix multiplications to get the field at 10^3 to 10^5 points throughout space.

Magnetization Surface Currents

Representation of magnetic elements by surface currents in ways that are most convenient for our software (arbitrarily oriented solenoids, wires, and planes) is rather straightforward. Consider a long magnetic cylinder of constant but small susceptibility χ in a uniform external B_0 with cylinder axis parallel to B_0 and χ equal to zero outside the cylinder. $B = \mu_0 H$ outside the cylinder. Inside the cylinder,

$$B = \mu_0(H + M) \qquad [11]$$

and M is constant.

The field B_S inside a solenoid in vacuum of length $l \gg r$ with n uniformly spaced turns of current i is constant, and it vanishes outside the cylinder:

$$B_S = \mu_0 ni/l \qquad [12]$$

To obtain the same internal field as the magnetic cylinder requires

$$\mu_0 ni/l = \mu_0 M = \chi B_0 \qquad [13]$$

Hence, a uniform solid paramagnetic or diamagnetic cylinder of susceptibility χ and length l aligned along the external field B_z is equivalent to replacing the cylinder with a solenoid coincident with the cylindrical surface with ni amp-turns, where

$$ni = \chi B_0 l/\mu_0 \qquad [14]$$

By a similar argument, it is easy to show that the current density on the outer surface of a long hollow cylinder is the same as for the solid cylinder, and the inner surface has an equal current density in the opposite direction. The surface currents on the plane faces at each end of the cylinder are zero.

The above expression for the axially aligned cylinder is equally valid for any length of cylinder even though B is not uniform inside a short solenoid, and B is not zero outside the solenoid. This is reconciled by noting that in Eq. [11], M is constant (to first order), but H is not.

The more general expression for surface currents may be anticipated from Eq. [6] and the macroscopic model of Fig. 1. When the boundary is inclined with respect to the field, the surface current density is proportional to the projected length in the direction of the field. The current element di on each surface element may be calculated from the projected length of the area element in the field direction, $dl \sin\theta$, where θ is the angle between the field and the normal surface vector. The current element lies in the plane of the area element and is perpendicular to the external field:

$$di/dl = \chi B_0 \sin\theta/\mu_0 \qquad [15]$$

and a minus sign is required for inside surfaces. The general solution for the surface current density $\mathbf{J}(\mathbf{r})$ at the boundary between two regions of uniform magnetization $\mathbf{M}_1$, $\mathbf{M}_2$ can be shown to be

$$\mathbf{J} = \mathbf{n} \times (\mathbf{M}_1 - \mathbf{M}_2) \qquad [16]$$

where $\mathbf{n}$ is the unit vector normal to the surface and directed from region 1 to region 2.

It is also straightforward to calculate surface currents for the hollow cylinder rotated 90° so that its axis is perpendicular to the external field. For example, a cylinder aligned along the y axis with the magnetic field in the z direction has currents parallel to the y axis on the cylindrical surfaces. If these currents are represented by n equally spaced wires along the outside and n wires along the inside from the $-y$ end to the $+y$ end, the current in the wire at angular location θ and radius r is given by

$$i = 2s\pi\chi B_0 r \cos\theta/(n\mu_0) \qquad [17]$$

where s is -1 for an inside surface and $+1$ for an outside surface. The current density on the annular ends is constant ($ni = 2\chi B_0 r/\mu_0$), but for many thin-walled cylinders, it may be ignored if the region of interest is not near the ends.

Barbara has shown (*3*) that current on a cylinder of arbitrary orientation may be represented as the weighted sum of the surface currents calculated for a parallel cylinder and those for a perpendicular cylinder. That is, at each point on the surface,

$$\mathbf{J}_T = \mathbf{J}_1 \cos\phi + \mathbf{J}_2 \sin\phi \qquad [18]$$

where $\mathbf{J}_1$ is the current density for a parallel cylinder and $\mathbf{J}_2$ is the current density for a perpendicular cylinder.

Elliptical Symmetries and Demagnetization Factors

In the last section, we argued heuristically that the induction field inside an infinitely long cylinder of uniform magnetization aligned with $\mathbf{B}_0$ is uniform and equal to $\mu_0(\mathbf{H} + \mathbf{M})$, from which we determined the surface current density. By similar arguments, by direct calculations from Eqs. [10], [16], and [17], or by other methods (*7*), it is straightforward to show that the induction field inside an infinitely long uniform cylinder perpendicular to $\mathbf{B}_0$ is $\mu_0(\mathbf{H} + \mathbf{M}/2)$. For the uniform sphere, the uniform internal field is $\mu_0(\mathbf{H} + 2\mathbf{M}/3)$, and for the thin disk in the normal direction it is $\mu_0\mathbf{H}$. We say that the demagnetization field factor of the infinite parallel cylinder is 0, for the infinite perpendicular cylinder it is $1/2$, for the sphere it is $1/3$, and for the normal thin plane it is 1.

The above geometries are special cases or approximations of ellipsoids. It can be shown that the field inside any ellipsoid of uniform χ for any orientation with respect to a uniform B_0 is uniform (*7*). However, the internal field is highly nonuniform where the ellipsoid approximation is poor—near the edge of the thin disk, or near the ends of the long cylinder, for example.

It is often helpful to look at specific cases. Consider a long, vertical, cylindrical sample of water, which has a susceptibility of -9.05 E-6 (often denoted -9.05 ppm for convenience), inside a flat-bottomed glass tube ($\chi = -11$ ppm) aligned with a perfectly uniform external B_0 of 7 T. The field near the center of the sample will be reduced by 9.05 ppm, as the demagnetization factor for an infinite parallel cylinder is 0. From the expression for the field inside the finite solenoid, it is easy to show that the field on the top surface of the sample is $\chi/2$ (4.52 ppm) below B_0, which means if both the top surface and the central portion of the tube are in the sensitive region of the rf coil, the baseline width will be 4.5 ppm or about 1350 Hz without shimming. (It may take a longer than average rf coil to verify this, as the cylinder length needs to be about six times the diameter for the center δB to be within 1% that of the infinite cylinder.) Another implication of demagnetization factors is that the resonance of water in an isolated spherical bulb is displaced from the water resonance in a long tube by $\chi/3$, or 900 Hz at 7 T. But, of course, do not try to verify this with lock on.

Figure 3 illustrates the field contributions from the magnetism of the so-called magic cylinder, with radius to length ratio of $\sqrt{5}/4 \cong 0.56$. The field was calculated for an equivalent solenoid on the surface of the cylinder, as indicated by the closely spaced small circles. The software (see The FEA Approaches) indicates field direction and relative magnitude by directed line segments on a Cartesian grid. The length of the line segments is proportional to the square root (for increased dynamic range of the display) of the projected component in the display plane.

For the above aspect ratio, the demagnetization factor at the center is $1/3$, the same as for a sphere. Hence, the induced field inside a small spherical (Lorentzian) cavity at the center is zero, independent of the susceptibility of the cylinder. Although second-order gradients are nearly maximum for this condition and baseline width is about 3 ppm, fourth-order gradients are very small. Fourth-order gradients vanish for a radius to length ratio of $1/\sqrt{3} \cong 0.58$; hence, this aspect ratio is usually the easiest truncated sample to shim without susceptibility plugs, as Z^2 shims have an order ot magnitude more corrective range than Z^4 shims—at least for small samples.

The Magic Angle Cylinder

A particularly important nonellipsoidal case is the uniform finite cylinder with axis aligned at the magic angle with respect to $\mathbf{B}_0$. Being a finite cylinder, the fields are quite nonuniform, especially near the ends. However, as has been well known since Andrew's analysis of MAS in the late fifties, dipolar (hence, susceptibility) broadening within a sample may be averaged to zero by MAS, and the demagnetization factor is the same as for a sphere. A more complete analysis has been presented showing that perfect averaging of the z-component applies also to MAS within the field produced by a stationary finite magic angle cylinder (*3*). For example, a perfectly uniform concentric ring of a highly diamagnetic material (such as MgO) in the MAS stator near the sample may contribute as much as 4 kHz broadening in a high-field MAS probe nonspinning, but its contribution to the spinning linewidth is negligible (if precisely at the magic angle), and spinning sidebands are small for spinning speeds well above

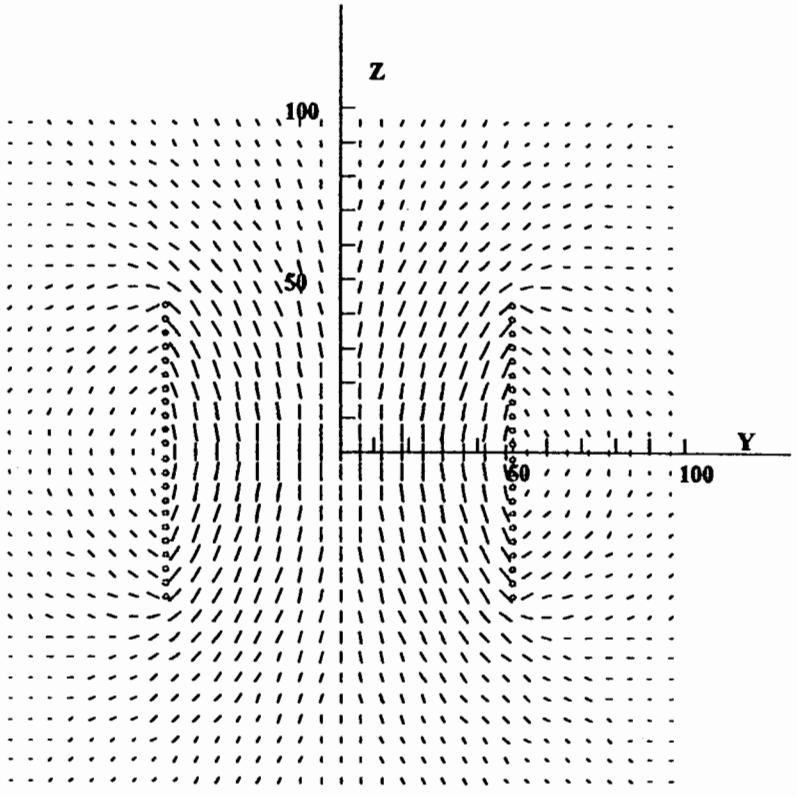

Figure 3 The field from the magic cylinder.

4 kHz. (Obviously, a 4-kHz static linewidth would not be acceptable in an HR MAS stator, as it should allow effective averaging at speeds as low as several hundred hertz.) We will return to more magnetism effects under MAS in later sections.

Types of Magnetisms

It is useful to briefly review the properties of the three main classes of magnetism: diamagnetism, paramagnetism, and ferromagnetism. Diamagnetism is associated with the tendency of electrical charges to partially shield the interior of a body from an applied magnetic field and is present in all materials. The principle is related to Lenz's law: when the flux through a loop is changed, a current is induced to oppose the change. A simple classical derivation (*8*) gives the following expression for the diamagnetic susceptibility:

$$\chi_{d1} = -\frac{\mu_0 NZe^2}{6m}\langle r^2 \rangle \qquad [19]$$

where N is the number of atoms per unit volume, Z is the atomic number, e is the electron charge, m is the electron mass, and $\langle r \rangle$ is the effective orbital radius. Obviously, this diamagnetism is always negative, is not explicitly temperature dependent, and increases with atomic number. Examples where diamagnetism dominates include (in ascending magnitude) copper, silver, gold, cadmium, antimony, and bismuth. In the more complete quantum mechanical derivation (Van Fleck, 1932), a second term is added that depends on the matrix element of the z component of the orbital magnetic moment connecting the ground state and the excited state, which is sometimes large enough to make χ positive, as in aluminum and normal (β) tin. Current preference denotes this, too, as diamagnetism (*9*), as it is a quantum mechanical correction of the same effect, although it was originally called Van Fleck paramagnetism.

Paramagnetism is found in (a) free atoms and ions with a partially filled inner shell (transition elements), (b) molecules with an odd number of (or unpaired) electrons (such as O_2), (c) lattice defects with an odd number of electrons, (d) conduction electrons, and (e) nuclear spins. The first three of the above categories normally exhibit an inverse temperature dependence (Curie

law), given by:

$$\chi_p \cong \frac{\mu_0 N p^2 \mu_B^2}{3 k_B T}, \qquad [20]$$

where k_B is Boltzmann's constant, T is the temperature, N is the number of ions per unit volume, p is the effective magneton number, and μ_B is the Bohr magneton ($eh/4\pi m$) (*8*). Some of the highly paramagnetic ions (in descending order) include Dy^{3+}, Er^{3+}, Gd^{3+}, Fe^{3+}, Mn^{2+}, Fe^{2+}, Mn^{3+}, Cr^{2+}, Co^{2+}, Cr^{3+}, V^{2+}, Ni^{2+}, Pr^{3+}, V^{3+}, Ce^{3+}, Cu^{2+}, Ti^{3+}, and Sm^{3+}, with p ranging from 10.6 to 1.5.

The paramagnetism of conduction electrons is given by an expression that looks identical to Eq. [20], except that p is usually close to unity and T is replaced by T_F, the Fermi surface temperature, which ranges from about 1E4 K to about 2E5 K for various conductors and is nearly independent of the lattice temperature but often has a slightly negative temperature dependence. Hence, where conduction-electron paramagnetism dominates, susceptibilities are positive and usually nearly temperature independent but often increase slowly with temperature. Examples include (in descending order) Pd, V, Cr, Pt, Ti, Rh, Zr, Mo, Ta, W, and Hf. Nuclear paramagnetism (NMR) is three to eight orders of magnitude less than electron paramagnetism, and hence negligible in all magnetic design problems other than NMR by force detection.

Ferromagnetism

Ferromagnetism is the most familiar type of magnetism to the layman, but usually the least understood by NMR researchers. It is beyond the scope of this article to do much to remedy this state of affairs, as ferromagnetism and related spin orderings (antiferromagnetism, ferrimagnetism, etc.) are quite complex. However, we will denote a little more space to ferromagnetism—not because it is more often a problem in HR probe design (that claim belongs to diamagnetism), but because much of what is widely believed about ferromagnetism belongs in mythology. The defining attributes of ferromagnetism are that it retains a magnetization (remanence, B_r) in the absence of an applied field and its susceptibility may be extremely high, usually going through a maximum ranging from unity to 10^5 for an induction field between 0.01 and 2.4 T and dropping sharply as a saturation field or Curie temperature T_C is approached.

In paramagnets at normal temperatures, Boltzmann statistics (thermal agitation) results in only a small fraction ($\sim 10^{-3}$ for electrons) of the spins aligning with the field. In ferromagnets, a fictitious exchange field B_E of the order of 1000 T is postulated that maintains complete (or nearly complete) spin alignment within domains up to the Curie temperature T_C for low applied fields (*7*). "Hard" ferromagnets are characterized by high coercivity (the intensity H_C required to return B_r to zero), low permeability, nearly square hysteresis (B-H retrace) loops, and small domain size. The opposite is true of "soft" ferromagnets, where domain size may be as large as 0.1 mm and permeability as large as 10^5. At temperatures above T_C (627 K for Ni, 1043 K for Fe, and 1388 K for Co), the exchange field B_E vanishes and ferromagnets look like superparamagnets with susceptibility inversely proportional to the temperature, though still very high below saturation. At fields above saturation (0.48 T for Ni, 1.7 T for Fe, and 2.35 T for CoFe), χ is < 1 and decreases inversely with field. The saturation magnetization decreases rapidly as the temperature approaches T_C.

In addition to the common ferromagnetic alloys (Fe-Co-Ni-Mn), there are dozens of ferromagnetic compounds with T_C above 300 K. Some of these (in descending order of T_C) include $FeOFe_2O_3$, $NiOFe_2O_3$ (T_C = 858 K), $CoOFe_2O_3$, Mn_4N, $CuOFe_2O_3$, Cu_2MnAl, MnBi (T_C = 630 K), CrO_2, $GdMn_2$, etc. In the class of antiferromagnets, the spins are ordered in an antiparallel pair arrangement below the Neel temperature T_N for one direction of the applied field. As a result, for this orientation at low fields, their susceptibility increases (sometimes rapidly) up to T_N and then decreases—much like a ferromagnet. At high fields, their behavior resembles superparamagnets. Examples (in descending order of T_N) include CrSb, NiO (T_N = 525 K), MnTe, Cr_2O_3 (T_N = 307 K), CoO, FeO, $CuCl_2$, and $NiCl_2$ (T_N = 50 K).

The exchange field is a short-range interaction that decreases rapidly as the distance between the potentially ferromagnetic atoms is increased. For example, since copper and nickel are completely miscible in all proportions in the solid state as well as the liquid state, as copper is added to nickel, its T_C decreases essentially linearly from 627 K at 100% Ni to 273 K at 68% to 0 K at 43.5% Ni (*10*). As chromium is added to iron, its

T_C decreases to 900 K at 75% Fe. A common austenitic stainless steel, type 316 L (65Fe-17Cr-12Ni-2.5Mo-2Mn-1Si-0.03C), usually has T_C below 1 K, so its normal behavior is highly paramagnetic.

While the austenitic stainless steels are perfectly acceptable for magnet cryostats and constant-temperature probe cryostats and probe dewars that extend at least 100 mm in both directions from the center of field, lower-susceptibility alloys are required for most other HR dewars. Of course, many probe manufacturers use glass dewars within its allowable temperature range, but where space is extremely limited, this is not an option. A nickel alloy with rather low magnetism and very low conductivity, often chosen for probe dewars, is Haynes Hastelloy C-22 (60Ni-22Cr-13Mo-3W-3Fe-2Co) (*11*).

Easily brazeable alloys such as C715 (67Cu-31Ni-0.5Mn-0.5Fe) (*12*) are not only easier to work with but also make better dewars because of their lower outgassing and magnetism. A Cu-Ni-Al-Cr-Mo alloy (similar to C719) is currently under development that has an order of magnitude lower susceptibility than alloy C715 but similar properties otherwise (*13*). Other CuNi alloys for susceptibility compensation applications are discussed later.

From an NMR high-field probe design perspective, one is generally concerned only with the possibility of contamination of materials near the sample by ferromagnetics. Because iron and cobalt are essentially insoluble in copper, there is the potential for the formation of ferromagnetic centers in copper by precipitation of one of these contaminates even when present at only 25 ppm —the maximum Fe level in C10100 copper, although the typical impurity levels are under 4 ppm Fe and under 0.2 ppm Co in oxygen-free high conductivity (OFHC) copper. While this may present problems in very-low-field HR probes, in high fields it is never a problem—since $\chi \sim 2/B_0$ tesla. Even standard brass alloys (CuZn or CuSn) with maximum iron content of 0.35% do not usually present problems in structural components relatively close to the sample in high-field probes, as the iron content is usually lower than specified by a factor of three and bound up in stable Sn-rich or Zn-rich phases, which are not ferromagnetic. Also, the beryllium-copper alloys, which are strengthened by precipitated beryllides (*12*) of (Cu, Co) and (Cu, Ni) and may contain over 0.1% Fe, have negative susceptibility above 5 T at room temperature. There are, of course, copper alloys strengthened by precipitation of Fe-rich manganese and aluminum compounds that are quite ferromagnetic, and these ferromagnetic compounds may form in alloys where their concentrations are rather low. However, highly paramagnetic phases are more likely to occur. For ferromagnetism to occur, the dilute alloy must be held at a moderately high temperature long enough for supersaturated ferromagnetic phases to precipitate and diffuse to the grain boundaries, where they can concentrate sufficiently for ferromagnetic exchange fields to become effective. Ferromagnetism in copper is much more likely to result from surface contamination by ferromagnetic cutting and forming tools of insufficient hardness. Cutting tools used on critical rf coils must be of a ceramic, a nickel-based superalloy such as U720, a hard titanium alloy such as Beta-C, or a high-speed steel (ferritic Fe-Mo-Cr-Co-W-C alloys with high abrasion resistance).

We have never found the common aluminum alloys (6061, 6063, etc.) to be ferromagnetic, as the iron is usually lower than the maximum specs (0.7% and 0.3%, respectively) by a factor of three and bound up in Al-rich phases. In fact, these alloys have susceptibilities very close to that of pure aluminum, as the diamagnetism of their magnesium and silicon components offsets the paramagnetism or antiferromagnetism of the iron compounds.

SUSCEPTIBILITY MEASUREMENTS AND CALCULATIONS

To most mechanical and electrical engineers, a material with magnetic susceptibility χ below 0.05 at low field is nonmagnetic, as it normally exhibits negligible magnetic attraction—at least, compared to iron. However, even the casual NMR probe builder knows that a chip of a high-energy Nd-B-Fe permanent magnet will exhibit a relatively strong attraction to such things as stainless steel, most o-rings, and some ceramic capacitor dielectrics. The susceptibility detection threshold for the magnet-on-a-string technique is about 100 ppm—which, fortunately, is adequate in screening for ferromagnetism, since this test is made at several tenths of a tesla and the end use will be at a field 20–100 times higher, where ferromagnetic susceptibility will be reduced by two to four orders of magnitude. However, three orders of magnitude better sensitivity in susceptibility measurement is required for diamagnetic

and paramagnetic materials, as their susceptibility usually has little field dependence.

Commercial, low-cost susceptibility balances, operating at 0.3 to 0.4 T (based on force balance in a high-gradient field), are supposed to have 0.01 ppm sensitivity, but our experience with a moderately priced commercial magnetometer has been unsatisfactory. We found it extremely difficult to get reproducibility within 10 ppm. Apparently, static charges in dielectrics could result in errors of 100 ppm at times. Moreover, there is no reliable method of relating this low-field measurement to high-field susceptibility if the ferromagnetic and antiferromagnetic components are unknown.

Published susceptibility data for modern engineering materials have not generally been available; and if available, they are often unreliable. The susceptibility of a conductor may have been determined by a vibrating magnetometer without proper consideration of eddy current effects, and purity is seldom adequate in ceramics for reliable measurements of diamagnetism at low fields, where ferromagnetic components must be below a fraction of a part per million. Even published values of the susceptibilities of such standards as pure copper and pure aluminum during the past 2 decades vary by more than 3%.

Several methods of using an NMR probe to determine high-field susceptibility from the shift or linewidth that is produced by a magnetic test piece at a particular position relative to the rf coil and a known NMR sample have been published (*2*, *14*, *15*), but we have developed a dual-ring NMR technique that we find more reliable, especially for conductors.

The Dual-Ring Susceptibility Measurement Technique

Our technique incorporates two identical rings of material to be tested, placed coaxially and at equal distance above and below the active NMR sample region as shown in Fig. 4. This arrangement gives a very homogeneous magnetic field at the sample region, similar in concept to Helmholtz coils.

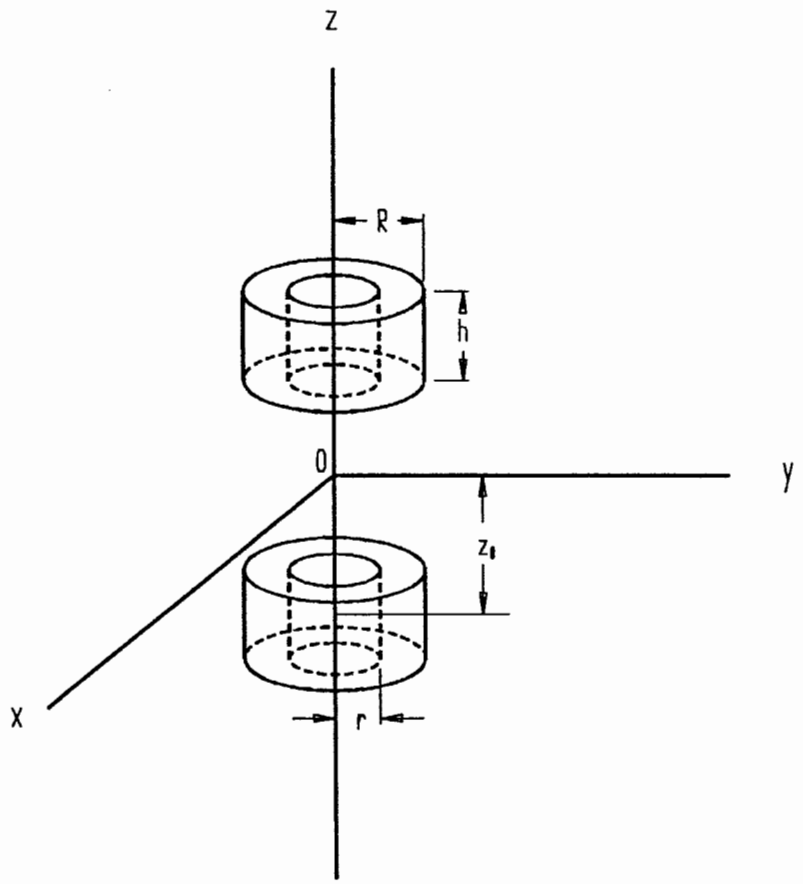

Figure 4 Dual-ring susceptibility measurement method.

To illustrate this point, we choose the cylindrical coordinate system so that the origin is at the center of the sample, and the z axis is along the B_0 field. Suppose the two rings have susceptibility χ, outer radius R, inner radius r, and length h; they are placed at $+z_0$ and $-z_0$, respectively, along the z axis. Using Eqs. [10] and [14] or [16], the induced magnetic flux density along the z axis can be calculated analytically, since the components perpendicular to the z axis cancel out and only B_z remains. The induced field by the lower ring is

$$\mathbf{B}_1(z) = \frac{\chi}{2} B_0[F(z, -z_0, R) - F(z, -z_0, r)]\mathbf{e}_3 \qquad [21]$$

where

$$F(z, -z_0, R) = \frac{z + z_0 + \frac{h}{2}}{\sqrt{\left(z + z_0 + \frac{h}{2}\right)^2 + R^2}} - \frac{z + z_0 - \frac{h}{2}}{\sqrt{\left(z + z_0 - \frac{h}{2}\right)^2 + R^2}}$$

and a similar expression for $F(z, -z_0, r)$.

Similarly, the induced field by the top ring is

$$\mathbf{B}_2(z) = \frac{\chi}{2} B_0[F(z, +z_0, R) - F(z, +z_0, r)]\mathbf{e}_3 \qquad [22]$$

while the field induced by both rings is the addition of the two,

$$\mathbf{B}(z) = \mathbf{B}_1(z) + \mathbf{B}_2(z) \qquad [23]$$

Taking the z derivative of the F function,

$$\left.\frac{\partial F(z, -z_0, R)}{\partial z}\right|_{z=0} = \frac{R^2}{(z_0 + h/2)^2 + R^2} - \frac{R^2}{(z_0 - h/2)^2 + R^2} \neq 0$$

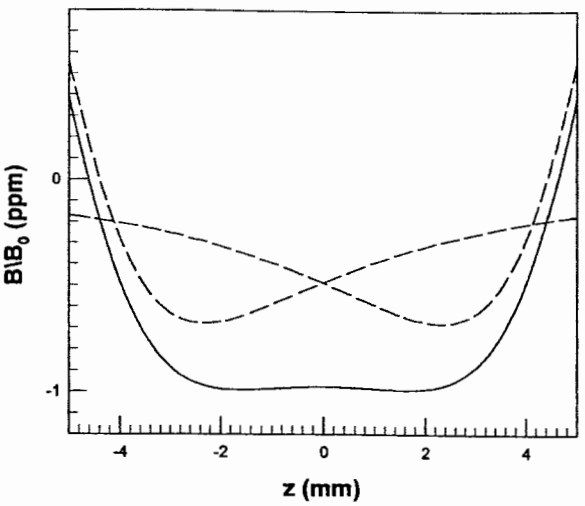

Figure 5 Field plots for the dual-ring method.

However, it is easy to verify that

$$\left.\frac{\partial F(z, -z_0, R)}{\partial z}\right|_{z=0} + \left.\frac{\partial F(z, +z_0, R)}{\partial z}\right|_{z=0} = 0$$

Hence, while each ring creates a strong z gradient at the center of the sample region, the combined field has no first-order z gradient at the center region.

Figure 5 demonstrates this point more clearly. The plot is obtained by numerical calculation of Eqs. [21–23], with the parameters $R = 4.99$ mm, $r = 2.56$ mm, $h = 5.00$ mm, $z_0 = 7.8$ mm (all data are actual dimensions used in measurements), and $\chi = -9.6$ ppm (copper). The dotted lines are the fields created by each respective ring while the solid line is the combined field. We see that the combined field doubles the strength (hence, measurement sensitivity) while it minimizes the field gradient at the same time. Consequently, the two-ring setup gives minimal line distortion, and as long as the sample window is kept relatively short (either by limiting the sample with susceptibility matched plugs as described in a later section, or by shielding the sample outside the window with thin foil, preferably susceptibility compensated), the measurement result is insensitive to the accuracy of sample positioning. For example, a ± 1-mm misplacement of the rings relative to the sample would give $\sim \pm 0.9\%$ error in susceptibility measurement in the two-ring configuration, while the same misplacement for a single ring would give $\pm 21\%$ error.

In practice, we use a 5-mm sample tube with a 10-mm HR probe to perform the measurements. The average induced magnetic field within the sample volume is calculated using our in-house electromagnetic (EM) modeling software, COILS. The dimensional parameters are chosen so that the rings fit snugly between the 5-mm tube and the 10-mm probe.

High-Field Susceptibility of Engineering Materials

Tables 1 and 2 list some susceptibility data for important NMR probe engineering materials at 300 K, 7 T as measured by the method described above. The dielectric loss data are also original. The method used to obtain this data will be described elsewhere. The rest of the properties are collected from a number of sources—especially (*5*), (*8*), and (*12*). The temperature and field dependence of the susceptibilities of the materials listed is generally rather low (at least for fields above 4 T and temperatures above 50 K), except for SS316, C-22, C1751, C715, Pd, and the Ni-Cr-Co-Ti superalloy Udimet-720, which, like the hard titanium alloy, is useful in high-pressure probes and critical tooling.

The FEA Approaches

Over a dozen commercial EM modeling software packages are available that can handle some of the magnetism problems in NMR and magnetic resonance imaging (MRI) probes. A typical package usually contains three parts: a "preprocessor," which is used to draw the objects to be modeled and defines boundary conditions and/or sources; one or more "solver(s)" that calculate the fields and currents using special cases of Maxwell's equations within the boundary, until they satisfy the required accuracy; and a "postprocessor" that calculates derived parameters and generates numerical or graphical outputs. The cost for such a package ranges from around $12,000 [usually includes one two-dimensional (2D) solver] to over $40,000 (includes several 2D and 3D solvers).

Most of the commercial software uses finite element techniques. It requires the entire volume of the configuration to be meshed, as opposed to surface integral techniques (sometimes also re-

Table 1 Properties of Probe Metals at 300 K, 7 T

Material	Density	Electrical Conductivity	Thermal Conductivity	Thermal Expansion	Specific Heat	Magnetic Susceptibility
Symbol	d	σ	k_T	b_T	C_P	χ
Units	kg/m^3	M$(\Omega$m$)^{-1}$	W/mK	10^{-6}/K	J/kgK	10^{-6}
Aluminum	2700	36.6	230	22.0	900	20.9
Al-6061T6	2700	25.0	180	23.6	896	19.5
Copper	8950	58.0	400	16.5	490	−9.6
C1751-HT	8830	30.0	240	18.0	500	−5.0
C510 CuSn	8860	11.5	84	17.8	380	−10.0
C715 CuNi	8940	2.6	29	16.0	380	790
Haynes C-22	8690	0.9	10	12.4	414	590
Gold	19,300	44.0	315	14.2	128	−34
Hafnium	13,090	2.9	22	5.9	145	69
Iridium	22,500	19.8	147	6.8	130	38
Molybdenum	10,200	18.1	138	5.2	276	120
Palladium	12,020	9.3	76	11.8	245	840
Platinum	21,450	10.6	71	9.1	132	279
Rhodium	12,440	20.9	150	8.3	247	168
Silver	10,500	61.4	428	19.0	235	−24
SS316L	8000	1.4	16	16.0	500	2800
63/37-SnPb	8340	6.8	50	22.0	176	−3.5
96/4-SnAg	7500	8.2	70	20.0	220	0.6
Ti (β-C)	4820	0.7	8	8.7	450	270
Tungsten	19,250	18.4	173	3.8	133	80
Udimet 720	7900	0.7	18	13.5	430	540
Zirconium	6506	2.3	21	5.85	295	160

Table 2 Properties of Probe Dielectrics at 300 K

Material	Density	Dielectric Loss* ~ 500 MHz	Thermal Conductivity	Thermal Expansion	Specific Heat	Magnetic Susceptibility at 7 T
Symbol	d	tan δ	k_T	b_T	C_P	χ
Units	kg/m^3	%	W/mK	10^{-6}/K	J/kgK	10^{-6}
Al_2O_3	3950	0.02	35.0	8.0	780	−14.0
Aurum-Pl	1330	0.19	0.18	55.0	1000	−8.9
A-JGN3030	1560	0.30	0.30	~ 35	960	−6.5
Epoxy 353ND	1200	4.0	0.20	54.0	1400	−11.5
Kel-F	2100	2.8	0.21	60.0	800	−11.6
Macor	2520	~ 0.1	1.7	9.0	750	−11.7
MgO	3400	~ 0.1	20.0	13.5	955	−17.8
PEEK	1300	0.40	0.24	54.0	1500	−9.3
PPS	1350	0.22	0.20	50.0	~ 1200	−9.2
Pyrex-7070	2500	~ 0.2	1.3	3.3	800	−11.0
Quartz	2250	0.03	1.4	0.5	700	−11.8
Silicone	1080	0.25	~ 0.3	~ 30	1800	−7.8
Si_3N_4	3250	0.09	25.0	3.2	740	−14.0
Teflon	2200	0.05	0.25	120.0	750	−10.5
Ultem–PEI	1270	0.18	0.30	55.0	1300	−9.0
Vespel	1430	0.30	0.33	54.0	1130	−9.2
Water	997	~ 5	0.60	—	4182	−9.05
Zirconia (Mg)	5700	~ 0.2	3.0	9.5	490	−8.8

* Loss tangent data measured at ~ 400 K, ~ 400–600 MHz.

ferred to as moment methods), which only require the surfaces to be meshed. Finite element methods excel at modeling complex inhomogeneous geometries, since each mesh element may have completely different material properties from those of neighboring elements. However, they do not model unbounded, homogeneous problems as effectively as surface integral methods. It is particularly time-consuming to model a configuration whose largest dimension is larger than its smallest dimension by two orders of magnitude or more, as the number of mesh elements needed increases dramatically as this ratio increases. For example, it takes several hours on a 200-MHz Pentium Pro computer to solve the fields of a thin-wall, long cylinder with several chip capacitors attached around its outside perimeter inside a homogeneous B_0 field. Since most of the NMR magnetism problems we face are of similar configurations, we found it more efficient to use the surface integral method—which is one of the reasons behind the development of COILS.

Biot-Savart-Based Software: COILS

Over the past 4 years, we have developed Windows-based Biot-Savart software called COILS for modeling and optimizing the effects of current distributions comprised of common winding geometries, especially for NMR gradient applications. Its adeptness at handling cylindrical surface current densities makes it relatively easy to model the effects of magnetic susceptibility, especially for cylindrical symmetry parallel or perpendicular to the external field. Arbitrary magnetic geometries can also be accommodated, although it becomes rather laborious in most cases. The code is particularly efficient in handling variations in a complex system. Recalculations typically take only a few seconds to a few minutes on a Pentium-200, depending on the extent of the changes.

Only a brief overview is presented here, as more detailed documentation is furnished with the software, which is available at a modest price (*13*). A magnetic cylinder would be modeled as a solenoid covering its surface with n closely spaced turns of wire. In addition to calculating the field and gradients, it calculates the resistance and power for this fictitious conductor, which is specified as a superconductor since it is lossless. The number of turns is arbitrary as long as ni is correct. The sample region for homogeneity analysis by COILS may be either a sphere or a cylinder aligned with the z axis.

Even though the magnetic field at which we usually check our modeling is 7.05 T and the final application may be at some other field, it is usually easiest to do the modeling at 1000 T. With the output in mT, inhomogeneity in ppm is then simply the variation in the field generated by the magnetic materials throughout the sample region. Many of the parameters it calculates for real coil systems (inductance, resistance, filling factor, etc.) are meaningless for magnetism modeling.

Several simple preprocessors were written (a) to perform the calculation of *ni* for a magnetic cylinder parallel to the external field, (b) to calculate the coordinates and currents of longitudinal lines on the surface of a cylinder perpendicular to $\mathbf{B}_0$, or (c) to calculate the transverse current lines on the disks on the end of perpendicular cylinders.

SUSCEPTIBILITY COMPENSATION TECHNIQUES

We saw in Elliptical Symmetries and Demagnetization Factors that BMS in truncated samples could easily make unshimmed baseline widths two orders of magnitude larger than is sometimes needed in HR NMR. The simplest solution to this problem is to use very long samples and high-performance shims. Of course, samples are often limited, and there are limits to what shims can do, as we will see later.

The spherical sample bulb is often an excellent solution for improving S/N with limited samples by reducing the solvent volume and hence increasing concentration within the active coil region, but it has its limitations: (a) The stem is not normally magnetically compensated and hence produces severe inhomogeneities near the top of the sample; (b) the fine stems needed to minimize perturbations make sample loading difficult; and (c) the length of the active coil region is often three times the inside diameter of the sample tube, which means the spherical cell volume (it must fit inside the tube) is typically under 12% of the normal sample tube active volume, which may be too small when solubility is limited. Of course, the deleterious effects of the stem may be reduced by immersing the bulb in a highly diamagnetic liquid (such as chloroform), or a paramagnetic wire (such as aluminum) of the right size inside the stem can help even more (as we will see in Copper-Clad Compensated Wire and Foil), but susceptibility-matched sample plugs are often a better solution.

If samples themselves can cause enormous BMS effects, what about the rf coil and associated hardware? It should be obvious by now that special attention must be paid to both symmetries and materials in the probe construction, especially those very near the sample. While the rf coilform either for a transverse solenoid or for an axially aligned saddle coil can often be made long enough for negligible perturbation in the sample region (since the central region of the tube may be approximated by two long, concentric ellipsoids), one has to worry about magnetic compensation of any holes that may be required in the coilform near the sample for leads, capacitors, or air flow.

Magic symmetries are not generally an option for the rf coil. Thus, it must be made either of extremely thin foil or of a material of zero net magnetization. The same applies to coil adhesives. The following sections address these magnetism issues in more detail.

Susceptibility-Matched Plugs

High-resolution NMR has normally required a sample length that extends above and below the edge of the rf region by at least the sample diameter because it is impossible to shim out the near-field effects of a magnetic susceptibility discontinuity except for a few special symmetries. The newer shim systems would allow a slight reduction in excess sample length, except that line-shape standards are becoming more strict.

Plugs matched to the solvent's susceptibility within 5% eliminate the need for 70% of the excess sample and allow sensitivity to be increased because of higher concentration (*16*). When the susceptibility mismatch is about 0.5 ppm (SI), the sample need extend only several millimeters beyond the active region. When the plugs are matched within 0.1 ppm, the plug–sample interface may lie *within* the active region with no significant loss in resolution. Moreover, line shape and resolution (especially in older probes) may be improved, as poor line shape in older probes arose mostly from poor confinement of the rf to the central sample region—it is usually impossible to achieve ultra-high homogeneity over more than the central 18 mm of sample length.

Another important reason for susceptibility-matched plugs occurs with large samples of low

Table 3 Susceptibilities and Densities of Common Solvents

Solvent Name	Formula	Mol. Wt. (kg/mol)	Density (g/cm^3)	$-\chi_C$ (cgs) (20°C)	$-\chi$ (SI) (20°C)
Glycerol	$C_3H_8O_3$	92.1	1.26	0.78	9.80
Bromo-benzene	C_6H_5Br	157.0	1.50	0.75	9.43
Chloroform	$CHCl_3$	119.4	1.48	0.74	9.30
Trichloroethylene	C_2HCl_3	131.4	1.46	0.73	9.18
Water	H_2O	18.0	0.997	0.72	9.05
Deuterium oxide	D_2O	20.0	1.10	0.70	8.80
Carbon disulfide (22°C)	CS_2	76.1	1.25	0.70	8.80
Carbon tetrachloride	CCl_4	153.8	1.58	0.69	8.67
Cyclooctane	C_8H_{16}	112.2	0.85	0.68	8.55
DMSO	$(CH_3)_2SO$	78.1	1.10	0.66	8.30
Cyclohexane	C_6H_{12}	84.2	0.77	0.63	7.92
Toluene	C_7H_8	92.1	0.86	0.62	7.79
Benzene	C_6H_6	78.1	0.87	0.61	7.67
Dioxane (32°C)	$C_4H_8O_2$	88.1	1.03	0.61	7.67
Nitro-benzene	$C_6H_5NO_2$	123.1	1.20	0.60	7.54
Isopropyl alcohol	C_3H_8O	60.1	0.80	0.60	7.54
Ethyl alcohol	C_2H_6O	46.1	0.79	0.58	7.29
Acetic acid (30°C)	$C_2H_4O_2$	60.0	1.04	0.55	6.91
(Di)ethyl ether	$(C_2H_5)_2O$	74.1	0.71	0.53	6.66
Methyl alcohol	CH_4O	32.0	0.79	0.53	6.66
Methyl ethyl ketone	C_4H_6O	72.1	0.80	0.51	6.41
Acetone	$(CH_3)_2CO$	58.1	0.78	0.46	5.78
Ethylene glycol	$C_2H_6O_2$	90.1	1.11	0.40	~ 5

solubility. Thermal gradients as small as 0.1°C in larger nonspinning sample tubes (even 8 mm) can drive sample convection and may cause serious spectral artifacts (*17*). Reducing the sample length by a factor of three using susceptibility-matched plugs may not be sufficient to prevent convection; but if convection occurs, the spins remain confined to the active B_1 region during the acquisition period. Slow spinning suppresses convection; but for nonspinning VT HR-NMR, susceptibility plugs are often required.

Table 3 lists susceptibility data on a number of solvents in both cgs volumetric and SI volumetric units, and Table 4 provides technical information on susceptibility plugs that are available from Wilmad, as illustrated in Fig. 6 (*18*). A variety of

Table 4 Plug Materials: Susceptibility and Chemical Compatibility

	Kel-F	PPS	Aurum	Ultem	Zirconia	GFP	G-10
χ_C (ppm, cgs)	0.92	0.73	0.71	0.71	0.70	0.52	~ 0.5
Wideline NMR backgrounds	F, Cl, C	H, C, S	H, C, N	H, C, N	Zr	H, C, Al, Si, F	H, C, Al, Si, F
H_2O absorp. (%)	0.02	0.03	0.80	0.70	0.01	0.20	0.15
Density (g/cm^3)	2.10	1.35	1.42	1.27	5.70	1.45	1.88
Max use T, (°C)	150	120	240	205	700	250	160
Color	Clear	Ivory	Black	Amber	White	Gray	Green
Chemical Resistance							
Strong acids	E	G	G	G	E	P	F
Strong bases	E	E	G	G	E	G	E
Alcohols & aliphatics	E	E	E	E	E	E	E
Aromatic H-C	E	E	E	G	E	E	E
Esters & ketones	E	E	E	E	E	E	E
Chlorosolvents	E	E	G	F	E	G	G

E = excellent; G = good, usually acceptable; F = fair, sometimes acceptable; P = poor.
Volumetric suscept. χ in S.I. is related to vol. suscept. χ_c in cgs by: $\chi = 4\pi\chi_c$.

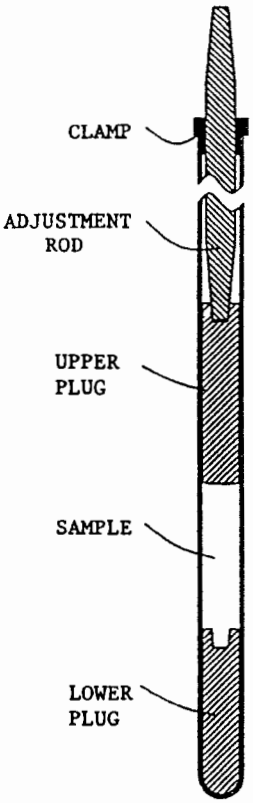

Figure 6 Early version of the Doty susceptibility plugs.

plug materials is required to match to a wide range of solvents without introducing broad background signals. Low moisture absorption is often quite important, as absorbed water is broad and difficult to suppress. Polyphenylene sulfide (PPS) is particularly good in this respect, although its homogeneity is not as good as that of the other materials. Other available material include Kel-F [polychlorotrifluoroethylene, G-10 (60% e-glass epoxy composite], aurum (thermoplastic polyimide), ultem (polyetherimide), GFP (glass-filled polyetheretherketone), and CPVC (chlorinated polyvinylchloride). Specially formulated glass tubes with attached plugs in several susceptibilities are available from Shigemi.

Copper-Clad Compensated Wire and Foil

Since the first superconducting magnets in the early 1970s, rf coils in HR probes have usually been etched from thin foil (rather than formed from copper wire) for three compelling reasons: B_0 homogeneity, B_1 homogeneity, and radial space constraints. At high fields, the proton coil is normally a slotted resonator (*19*), an Alderman–Grant segmented slotted resonator (*20*), or a split-half-turn saddle coil (*21*, *22*). The low-frequency coil has usually been a multiple-turn foil spiral (*23*), although multiple-turn wire coils are also frequently used (*1*). All of these rf coils (or resonators; the terms are used interchangeably) may be made from thin foil without loss in quality factor (for an inductor, $Q_{0L} = \omega L/R$) because of the rf skin depth effect.

Maxwell's equations prevent significant flux penetration of good conductors at high frequencies, which requires most of the rf current to flow close to the surface. For uniform plane waves near a flat conductor, the current density decreases exponentially into the metal with an attenuation constant given by the classical skin depth δ (*24*),

$$\delta = \left(\frac{2}{\omega\mu\mu_0\sigma}\right)^{1/2} \qquad [24]$$

where σ is the electrical conductivity. This amounts to about 3 μm in copper at 500 MHz, for example. Of course, the rf B_1 field is not a plane wave near the conductor foil edges. As a result, there is considerable current concentration at the edges (*25*). Some experiments suggest mean flux penetration of about 6δ on the edges of foil that is 6δ thick in slotted resonators, with skin depth gradually decreasing to the classical value away from the foil edges.

Since there is very little improvement in Q_{0L} as the conductor foil thickness increases beyond 6δ, the easiest way to minimize $\mathbf{B}_0$ perturbations from the rf coil is to use copper foil (copper is magnetically twice as good as silver) about $5–8\delta$ thick, as coils this thin minimize the total magnetic moment from this nonelliptical perturbation very near the sample without loss in Q. Figure 7 illustrates the $\mathbf{B}_0$ perturbations as calculated by COILS for just the conductive arcs (at 3.75-mm radius) and inner rf lead shields (at 3.0-mm radius) in an Alderman–Grant resonator using 60-μm copper foil (15δ at 300 MHz) with narrow (2.5-mm) conductor arcs. (The black-and-white copy fails to show the direction of the line segments, which are blue at one end and red at the other end in the computer display, so arrowheads were drawn in manually.) The coil is shown in Fig. 8. The z-component changes sign where the transverse components are maximum above and below these perturbations, as expected. The smooth 0.02-ppm variations in B_z over the central half of the sample can easily be shimmed to 1 ppb

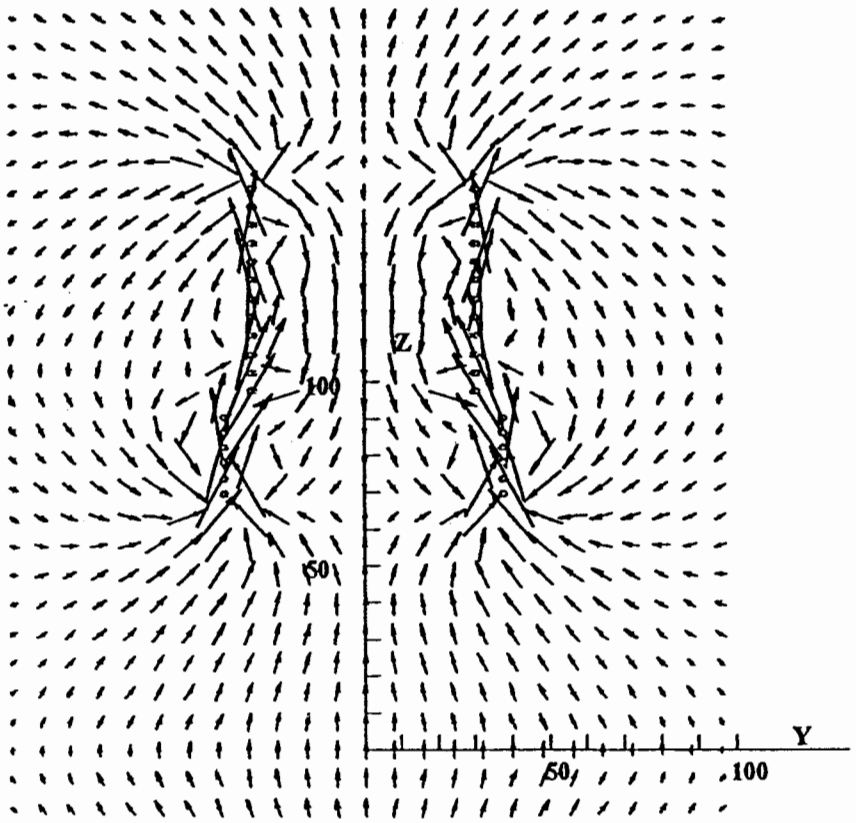

Figure 7 B_0 field from copper foil arcs and lead shields of a slotted resonator.

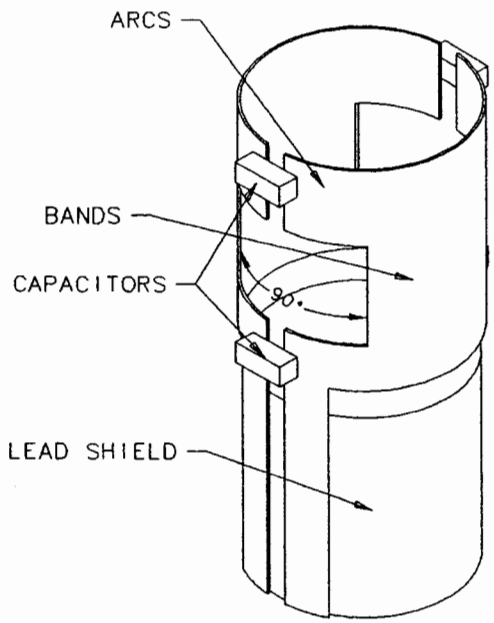

Figure 8 Alderman–Grant resonator with lead shields.

with just the even-order Z shims, but the shims have little effect on the high-order perturbations near the edges of the sample. The 0.04-ppm B_z perturbations near the edge of the sample (4.2 mm diameter) directly under the resonator arcs are in regions of low transverse B_1 (low sensitivity) and essentially determine the baseline width, which is about four times worse than desired for state-of-the-art high resolution in liquids. (Of course, this is much better than would ever be needed in MRI or solids.) The transverse component of B_1 is still reasonably large well inside the guard rings near the axis, where high-order shimming can be beneficial in reducing these 0.035-ppm contributions to the baseline width [see Fig. 6 in Fuks et al. (*2*) for a better 5-mm proton coil design, where 0.025 × 5-mm copper foil on an 8-mm tube without guard rings generates 30 ppb width at 0.5% amplitude in a 5-mm sample tube].

The Fuks example shows that 6δ may be enough copper foil thickness for three times the desired magnetic perturbations in HR NMR even at high frequencies with a relatively large distance between the sample and the coil, and there are

often reasons for choosing a much heavier foil or a closer coil spacing: (a) To handle the heating during high-power decoupling, the foil often needs to be at least 0.1 mm thick (at least 0.2 mm for NMR of solids); (b) sensitivity is improved by reducing the distance of the rf coil (to improve filling factor); (c) very thick foils are beneficial in stabilizing coil temperature (hence, Q_{0L}) during high-power pulses, which is critical in most 2D cancellation-type or inverse sequences; and (d) foils under 30 μm thick are rather fragile.

The earliest technique (*1*) for magnetic compensation of copper foil was to plate one side with rhodium such that the thickness ratio of rhodium to copper is $9.6/168 = 1/17.5$ according to the volumetric susceptibilities in Table 1. [Zelaya's experimental data (*26*) for Rh-plated copper cylinders give a volume ratio of 1/18, which may be more accurate]. Since the rf skin depth in rhodium is about 70% greater than in copper, its thickness would be about one skin depth when the copper foil thickness is about 3δ —a common situation in an inverse coil. When the external rf shield is well spaced from the rf coil, the mean current density on the inside is about twice that on the outside, so the Q is degraded by $< 30\%$ if the rhodium plating is on the outside. As the external shield gets closer (as when a gradient coil is needed) the current density on the outside increases and eventually exceeds that on the inside (for a shield diameter less than ~ 1.8 times the coil diameter), making it necessary to have good electrical conductivity on both surfaces of the foil. One method is to increase the rhodium thickness and then plate over it with 3δ of copper.

The susceptibility of copper, aluminum, silver, gold, and molybdenum are essentially independent of temperature and field (under 3% change between 70 and 500 K above 4 T) (*27*). On the other hand, rhodium, platinum, and iridium have +11%, −13%, and +18% changes in susceptibility, respectively, for this temperature increase, which makes perfect compensation over a wide range impossible using these materials. However, it is quite difficult to control plating thickness even within 15%, so the temperature coefficient is generally of secondary importance to plating accuracy. Field dependence is negligible above 4 T. Aluminum-plated foil is seldom practical—although it is possible with a zinc preplate.

There are still many situations where nonmagnetic wire (either round or partially flattened) is better than foil. Examples include saddle coils of more than two turns per side (*1*), solenoids, and high-impedance leads. Copper-clad aluminum wire is commercially available in diameters from 0.07 to 1.62 mm for industrial applications in electromechanical and electroacoustic transducers (*28*). The standard copper cladding is approximately 10% by volume, but its thickness is not precisely controlled, nor is the aluminum alloy composition. However, a Teflon coating of thickness about 30% of the wire diameter will give a total mean susceptibility close to zero, and custom plating ratios may be ordered. Since a slight improvement in Q is sometimes possible from silver plating, silver-plated aluminum wire has often been used by at least one major NMR vendor, even though magnetism control is extremely difficult and a high percentage of the wire must be rejected.

Very accurately compensated wire may be obtained by feeding aluminum wire through precision-extruded copper tubing, and wire of this type has recently become commercially available in various diameters from 0.53 to 1.62 mm (*13*). It may be plated with 0.1 μm of gold for corrosion protection with negligible effect on Q or magnetism. Normally, the goal is zero susceptibility rather than the susceptibility of air (0.4 ppm), as the wire is usually in a nitrogen atmosphere.

Quartz or silicon-nitride coilforms are normally used for minimum dielectric loss. If the coils are rigidly affixed to the coilform (see Coil Adhesives), the operating temperature range may be limited by the enormous stress from the differential thermal expansion between the foil or wire and the low-expression former. The thermal stress problem is worse with copper-plated aluminum (because of its higher thermal expansion) than with pure copper. Using iridium or tungsten-rhenium alloys rather than aluminum for magnetic compensation reduces the thermal stress in the ceramic-to-metal bond, since their low thermal expansion and high Young's modulus make it possible to more effectively limit the expansion of the copper (*29*). Such measures are necessary only for extended temperature ranges.

Copper-Nickel Alloys

The drawbacks of rhodium, platinum, or iridium plating are high cost and difficulty in plating and etching (chemical milling). Molybdenum is not expensive, but it is relatively brittle and the plating techniques are not well developed, although it may be possible to electroplate copper onto

molybdenum alloys (*30*). Copper-nickel alloys offer an attractive alternative.

As the nickel content is increased from 0% to 9%, the susceptibility of the annealed copper-nickel binary alloy at room temperature increases approximately linearly from -9.6 to $+16$ ppm (and the electrical conductivity decreases by a factor of eight). For higher nickel contents, the alloys have an increasingly negative temperature coefficient of susceptibility ($\sim -0.1\%/°C$ at 9% Ni) and the susceptibility varies by up to $\pm 5\%$ depending on the grain size and amount of work hardening. For nickel content above 22%, ferromagnetic impurities are more likely to form and the susceptibility becomes more variable. Considerable strengthening and some improvement in susceptibility stability may be obtained by minor additions (up to several percent) of aluminum and chromium and small amounts of molybdenum. It is important that the total Fe + Co + Mn content be $< 0.01\%$ and other highly paramagnetic elements such as titanium and vanadium also must be low for predictable and stable susceptibility. Several high-strength CuNiAlCrMo alloys with carefully controlled susceptibility are expected to be available in several foil thicknesses in the near future from an NMR probe vendor (*13*). The primary advantages of these alloys are their plateability, chemical milling properties (the copper-plated foil is easily etched using conventional methods for printed circuits), ductility, thermal expansion match to copper, strength, and low cost. Hence, they can easily be made very thin or thick enough for high-power solids decoupling applications without concern about delamination during severe thermal cycling (*29*). Their primary disadvantage is their low conductivity, which contributes to increased losses at the edges of etched foils.

Coil Adhesives, Substrates, and Coatings

A number of composite pulse techniques have been developed that are very effective in using the spatial inhomogeneity of the rf field to sharply limit spatially the size of the observed part of the sample for at least three purposes: (a) to improve line shape by ignoring signals from regions of the sample that cannot be well shimmed (*31*); (b) to reject probe background signals (*32*); and (c) for localized spectroscopy and imaging (*33*). Rejection of unwanted background signals can often exceed three orders of magnitude compared to a simple 90° pulse, and background subtraction may give another order of magnitude rejection. However, these techniques are not always adequate or convenient, and the sacrifice in sensitivity is often undesirable, especially when T_2 is very short. Hence, the probe builder is always concerned about background signals, especially from coilforms, coil adhesives, and capacitors. Usually, wideline signals are less troublesome than narrow backgrounds, as baseline correction algorithms add to the arsenal against broad backgrounds. Adhesive technology is as important as coil technology in HR NMR, as it is critical to backgrounds, $\mathbf{B}_0$ homogeneity, high-voltage, temperature range, and Q.

One method of avoiding the adhesive problem is direct metallization of the coilform. A thin silver film (about 0.1 μm) may be vacuum-deposited onto quartz or silicon-nitride tubes and then electroplated to a sufficient thickness (3–5δ) with copper, but the subsequent steps are difficult. The etch-resist polymer may be applied, exposed, and developed on an external cylindrical surface without too much difficulty, but internal surfaces are impractical. For thick coils, a compensating metal (rhodium) must be placed onto the coil after etching, and then another 3δ of copper or silver must be plated over the rhodium. Resistance in the thin foil coil exacerbates the plating control problems. Because of the number of difficult steps in this process, it is practical only for high-volume production of standard coils. Also, the Van der Waals adhesion in vacuum deposition is generally not sufficient to tolerate the severe thermal stresses from thick films on quartz at extended temperature ranges, and plated metals usually have more defects, and hence lower conductivity than annealed, rolled metals.

Many HR foil coils are etched onto copper-clad laminate (*23*) (such as kapton or glass-filled Teflon) and, if necessary, magnetically compensated prior to mounting on the former. Again, the adhesive problem may be avoided in some cases. For low-proton, copper-clad Ultralam (a glass cloth–reinforced Teflon) works very well unless low backgrounds are also required on fluorine, aluminum, sodium, or boron (glass fibers always contain these elements). (After etching and plating, absorbed water can be removed with a vacuum bakeout.) When cut precisely for a snug fit to the inside of a quartz tube, its rigidity will keep it firmly in place inside the tube even under severe thermal cycling without an adhesive. If the substrate is long compared to the sample, its susceptibility is immaterial if holes can be avoided.

Crossovers may be fed through fine slits so that magnetic perturbations are minimal. For low-fluorine probes, copper-clad kapton is often used. It usually requires an adhesive because its higher expansion will cause it to loosen under thermal cycling if a compression fit to the inside of a cylinder is attempted.

Often one of the best ways to secure an etched foil coil to the outside of a tube is with expanded heat-shrink Teflon tubing. Many commercial grades of Teflon give large proton backgrounds even after a vacuum bakeout, but several grades have negligible proton backgrounds after bakeout (Dixon Industries, Bristol, RI). If the expanded tubing is long compared to the sample and uniformly heated to 330°C, it will shrink with sufficient uniformity for high B_0 homogeneity, and it can be used repeatedly up to 260°C. For low-fluorine probes, heat-shrink polyolefin tubing may be used, but its temperature range and dielectric properties are inferior.

The wideline carbon signal from Teflon under one-pulse experiments often makes it necessary to minimize its use near the coil and leads in solids NMR. The use of a polymeric adhesive generally allows a reduction in total carbon compared to the use of heat-shrink tubing (even though the carbon density in Teflon is about one fourth that in epoxy) and may permit higher temperature operation. When narrow proton backgrounds are not critical, silicone adhesives are often the best choice for operation up to 250°C because of their low dielectric loss and elastomeric character. While the red room temperature vulcanizing (RTV) type is highly paramagnetic from iron oxide fillers, the common white and clear RTV commercial grades are generally acceptable, although they must be applied in extremely thin, uniform films to avoid serious magnetic perturbations. The RTV grades cure by a reaction with moisture in the air that produces acetic acid (hence, the characteristic vinegar smell). As a result, the cure is diffusion limited and proceeds quite slowly under wide traces of metal foils. In these cases, other adhesives are usually preferred.

The low-viscosity two-part heat-curing industrial silicones (such as Dow Corning 96-083) may be magnetically compensated by the addition of a combination of paramagnetic and antiferromagnetic powders such as Ti_2O_3, NiO, and Cr_2O_3 for nearly zero susceptibility over a reasonable temperature range. Unfortunately, the mobility of the ligands in silicone narrows its proton signal to about 700 Hz or less at room temperature. Addition of sufficient magnetic powder for zero susceptibility broadens the signal in proportion to the change in bulk susceptibility (*15*) to ~ 6 ppm, or 3 kHz at 500 MHz. Additional diamagnetic powder such as dry MgO can be added along with additional paramagnetic powder to broaden the background signal to about 12 ppm, but this is still too narrow for most proton applications. Moreover, dielectric loss is increased a little, as most highly paramagnetic compounds are not good dielectrics. Another difficulty that frequently arises with this adhesive is that the cure is inhibited by moisture or contact with many plastics, including the modified acrylic adhesive used in copper-clad kapton. However, when proton backgrounds are not critical, compensated silicone is often an excellent adhesive or coating material to control high-voltage arcing. Fluorosilicone adhesives have also been developed, but they are available only with highly magnetic fillers.

Rigid polystyrene is an ultra-low-loss rf dielectric at room temperature. It is soluble in toluene (and many other solvents) and is commercially available from electronic supply houses in this form under the trade name Q-Dope. When thoroughly dried, it makes an excellent coating for control of high voltage arcing at temperatures up to about 90°C, and its adhesion properties are also quite good despite its high shrinkage. It may be magnetically compensated in the same manner as the silicones, though with some loss in dielectric properties. Since its proton linewidth is around 20 kHz at room temperature, magnetic compensation has little effect in further reduction of the proton background signal. However, 99.9% deuterated styrene monomer is available from commercial isotope suppliers, which reduces the integrated background proton signal by three orders of magnitude, but low-level narrow lines appear. The same is true of polymethylmethacrylate (PMMA), which is also an excellent dielectric and usable up to 140°C at very low stress. PMMA is readily available dissolved in a volatile solvent in acrylic spray coatings and is very effective in controlling high-voltage arcing.

Many polyimides have dielectric loss lower than silicones at room temperature, and they are usually much better above 150°C. The thermoplastic polyimide aurum (Mitsui Toatsu Chemicals, Tokyo) has exceptional dielectric properties and is supposed to be capable of being used as a thermoplastic adhesive by applying moderate pressure to the parts while in a nitrogen atmo-

sphere at 360°C, but we have not thus far obtained satisfactory adhesion. Polyimide coatings (such as DuPont's Pyre-M.L.) have been widely used in the wire industry. They are initially soluble and may be precipitated from the solvent (perhaps with a very fine paramagnetic powder in suspension) onto a surface. A heat cure (usually above 250°C) then transforms them into a tough, insoluble coating. They make superior coatings for controlling high-voltage arcing, and one recently developed at NASA Langley Research Center (LaRC-SI) is reported to make an excellent adhesive in applications where the pressure, temperature, and solvent vapor can be properly controlled. It also may be relatively easy to synthesize from common perdeuterated precursors (*34*), but we have not yet developed reliable techniques for using this material as an NMR coil adhesive.

Finally, we come to epoxies—poor rf dielectrics, but excellent adhesives. We have found that some improvement in the rf power-handling capability of high-temperature epoxy Epo-Tek 353ND (Epoxy Technology, Billerica, MA) may be obtained by the addition of silicon nitride powder because of its high thermal conductivity and low dielectric loss. This loaded epoxy is usable to 350°C under conditions of moderate electric fields, but its high dielectric loss tangent will quickly cause burning when subjected to high-rf electric fields. However, when used sparingly, especially in regions of relatively low electric fields, the degradation in Q is often negligible up to 30 MHz and sometimes acceptable up to 800 MHz. Again, compensation with magnetic filler powders is necessary in HR probes if the epoxy is not being applied in long, thin, uniform films. Because of epoxy's high dielectric loss, there is less reason to worry about its degradation from the addition of a very lossy antiferromagnetic powder such as CuO, but compensation is usually poor if silicon nitride powders are added, as they are difficult to obtain with very low iron content.

Axial Density of Magnetic Materials in HR

As will be discussed in the next part, spinning in a supercon averages the odd-order transverse gradients very effectively and helps a little with the even-order transverse gradients. Thus, it is most important to minimize the high-order (unshimable) z-gradients generated by the rf coil. This was particularly true before the advent of z shims above fifth order, and it is still true even with nonspinning experiments. As discussed previously (*2*), the bands and guard rings in the conventional slotted resonator or Alderman–Grant resonator produce large Z^4 gradients within the central region and higher-order axial terms at the edges.

The field shown in Fig. 7 looks as though it were produced by two rings cut from a bar magnet and spaced apart along the z axis. If the coil instead were a uniform cylinder of the same overall length, the effects from the "magnetic charge density" on the inside edges of the rings would disappear (since these edges would be gone), and the field within the sample region would be much more homogeneous and largely quadratic in Z. Of course, it is impossible to make a transverse rf coil from a uniform copper cylinder.

Hill was the first to determine that for a spinning sample it is only necessary that the magnetization density along the z axis, when integrated around the spinning axis, be constant near the sample region for mean high-order axial gradients seen by the sample to be minimized (*35*). For example, this condition is met in a copper slotted resonator without guard rings, where the optimum subtended angle of the window is 90°, when the axial conductor bands are twice as thick as the rings (Fig. 8). Such a coil may be made from copper foil of uniform thickness by cutting and folding the window material back in flaps over the axial conductor bands rather than etching it away (*35*). (The electric-field guard rings are beneficial only for Alderman–Grant resonators on large samples.) However, this compensation method does little to improve nonspinning homogeneity, and line shape may be worsened. This method of compensation should be reserved for situations where compensated materials are not available and nonspinning line shape is not critical.

SUMMARY

We have reviewed some basic physics, properties, and types of magnetism as they relate to HR NMR probe design, both in liquids and in solids, and some of the reasons it is technically difficult to obtain resolution of several parts per billion. We noted the beneficial attributes of elliptical symmetries, susceptibility-matched sample plugs, and the finite magic angle cylinder; and some methods of calculating fields produced by various objects were reviewed, with emphasis on the method of effective surface currents. The magnetic properties, obtained by the dual-ring

method, of various materials important to NMR probe construction were presented, and methods of adjusting and controlling the susceptibility of special adhesives, wire, foil, and dewar alloys were discussed. Some preliminary results from the ongoing development of custom copper-nickel alloys, especially for NMR coil compensation and dewars, were also presented.

In Part II, we will look more specifically at HR MAS probe design issues, with particular reference to the Doty model XC5, where the requirements of fast variable-angle spinning and high-power decoupling must be integrated with magnetism, background, and VT requirements. Magic-angle positioning of B_0 perturbations, thermal gradients, and geometric compensation in the stator will be discussed along with some mechanical aspects of the spinner design. Equally important from a resolution perspective in solids is the capability of a long acquisition period under high-power decoupling. Some novel, high-frequency rf coils will be discussed for this purpose.

REFERENCES

1. D. I. Hoult, "The NMR Receiver: A Description and Analysis of Design," *Prog. NMR Spectrosc.*, **1978,** *12,* 41.
2. L. F. Fuks, F. S. C. Huang, C. M. Carter, W. A. Edelstein, and P. B. Roemer, "Susceptibility, Lineshape, and Shimming in High-Resolution," *J. Magn. Reson.,* **1992,** *100,* 229–242.
3. T. M. Barbara, "Cylindrical Demagnetization Fields and Microprobe Design in High-Resolution NMR," *J. Magn. Reson. A*, **1994,** *109,* 265–269.
4. F. D. Doty, "Probe Design and Construction," in *Encyclopedia of NMR*, Vol. 6, Wiley, New York, 1996, 3753–3763.
5. F. D. Doty, "Solid State Probe Design," in *Encyclopedia of NMR*, Vol. 7, Wiley, New York, 1996.
6. J. R. Reitz and F. J. Milford, *Foundations of Electromagnetic Theory*, Addison-Wesley, Reading, MA, 1967.
7. A Vlassenbroek, J. Jeener, and P. Broekaert, "Macroscopic and Microscopic Fields in High-Resolution Liquid NMR," *J. Magn. Reson. A*, **1996,** *118,* 234–246.
8. C. Kittel, *Introduction to Solid State Physics*, 4th ed., Wiley, New York, 1971.
9. D. L. VanderHart, "Magnetic Susceptibility and HR NMR in Liquids and Solids," in *Encyclopedia of NMR*, Vol. 5, D. M. Grant and R. K. Harris, Eds., Wiley, New York, 2938–2945.
10. M. Hansen, ed., *Constitution of Binary Alloys*, 2nd ed., McGraw-Hill, New York, 1989.
11. Haynes International, Inc., Kokomo, IN, 1988.
12. *Metals Handbook*, 10th ed., Vol. 2, ASM International, Materials Park, OH, 1990.
13. Doty Scientific, 700 Clemson Rd., Columbia, SC.
14. Kasten and R. Biehl, "Method for the Determination of Magnetic Susceptibilities," U.S. Patent No. 5,221,903, 1993.
15. J. A. Hopkins and F. W. Wehrli, "Magnetic Susceptibility Measurement of Insoluble Solids by NMR: Magnetic Susceptibility of Bone," *Magn. Reson. Med. 37,* **1997,** 494–500.
16. P. Zens, "Controlled Susceptibility Plugs," U.S. Patent No. 4,549,136, 1985.
17. J. Lounila, K. Oikarinen, P. Ingman, and J. Jokisaari, "Effects of Thermal Convection on NMR and Their Elimination by Samples Rotation," *J. Magn. Reson. A*, **1996,** *118,* 50–54.
18. F. David Doty and C. Vince Cothran, "Susceptibility-Matched NMR Sample Plugs," U.S. Patent Application No. 08/805,647, 1997.
19. H. J. Schneider and P. Dullenkopf, "Slotted Tube Resonator: A New NMR Probe Head at High Observing Frequencies," *Rev. Sci. Instrum.*, **1977,** *48,* 68–73.
20. D. W. Alderman and D. M. Grant, "An Efficient Decoupler Coil Design Which Reduces Heating in Conductive Samples in Superconducting Spectrometers," *J. Magn. Reson.*, **1979,** *36,* 447–451.
21. F. D. Doty, "Parallel Single-Turn Resonator for NMR," U.S. Patent No. 4,641,098, 1987.
22. F. D. Doty and Y. Yang, "HR MAS NMR Coils with Magic Angle Capacitors," patent pending.
23. P. Zens, "NMR Probe Coil System," 324/319, U.S. Patent No. 4,398,149, 1983.
24. F. D. Doty, R. R. Inners, and P. D. Ellis, "A Multinuclear Double Tuned Probe for Applications with Solids or Liquids Utilizing Lumped Tuning Elements," *J. Magn. Reson.*, **1981,** *43,* 399–416.
25. S. Crozier, K. Luescher, L. K. Forbes, and D. M. Doddrell, "Optimized Small-Bore, High-Pass Resonator Designs," *J. Magn. Reson. B*, **1995,** *109,* 1–11.
26. F. O. Zelaya, S. Crozier, S. Dodd, R. McKenna, and D. M. Doddrell, "Measurement and Compensation of Field Inhomogeneities Caused by Differences in Magnetic Susceptibility," *J. Magn. Reson. A*, **1995,** *115,* 131–136.
27. R. S. Tebble and D. J. Craik, *Magnetic Materials*, Wiley, London, 1970.
28. MWS Wire Industries, 31200 Cedar Valley Dr., Westlake Village, CA.
29. F. David Doty and George Entzminger, Jr., "Thermal Buffering of Cross-Coils in High Power NMR Decoupling," patent pending.
30. D. S. Lashmore and D. Kelley, "Process for Electrodepositing Metal on Tungsten, Molybdenum, and Other Difficult to Plate Metals," U.S. Patent No. 5,456,819, 1995.
31. Ad Bax, "A Spatially Selective Composite 90° RF Pulse," *J. Magn. Reson.*, **1985,** *65,* 142–145.

32. J. L. White, L. W. Beck, D. B. Ferguson, and J. F. Haw, "Background Suppression in MAS NMR," *J. Magn. Reson.*, **1992,** *100,* 559–566.
33. J. Shaka and R. Freeman, "Spatially Selective Radiofrequency Pulses," *J. Magn. Reson.*, **1984,** *59,* 169–176.
34. E. J. Siochi, P. R. Young, and R. G. Bryant, *40th International SAMPE Symposium*, Vol. 40, No. 1, 1995, p. 11. R. G. Bryant, personnel communication, 1997.
35. H. D. Hill, "Geometric Compensation of Magnetic Susceptibility Perturbations in an RF Spectrometer," U.S. Patent No. 4,563,648, 1986.

F. David Doty obtained his Ph.D. in physics at the University of South Carolina in 1983, where he worked on ESR instrumentation under C. Poole and H. Farach and on NMR instrumentation development under Paul Ellis. He and his wife Judy founded Doty Scientific, Inc., in 1982, in Columbia, South Carolina, where he continues as President and General Manager of Technology Development. He has over 20 publications and 25 patents in the areas of rf electronics, NMR probe technology, electromagnetism, manufacturing, turbomachinery, energy conversion cycles, ceramics, and acoustics. While his professional responsibilities keep him busy nearly 200% of the time, he still finds time to hike in the mountains or along the beach and to sing regularly with the church choir. His specific development projects constantly change with the interests of NMR customers.

George Entzminger, Jr. has worked as an electrical engineer with Doty Scientific, Inc., since 1986 immediately after receiving his B.S. in Electrical Engineering from the University of South Carolina. He is presently company Vice President and Service Manager for Doty and performs and evaluates many of the NMR probe development experiments. He has been doing hands-on work with NMR probes and techniques for the last 11 years. His work and ideas directly contributed to many of the features of the XC5 HR MAS probe.

Y. Andy Yang received his Ph.D. in physics from the University of Virginia in 1991, under the supervision of Louis Bloomfield. His graduate research involved the study of molecular clusters by means of mass spectroscopy and photoelectron spectroscopy. He joined Doty Scientific, Inc., in 1994. His current focus is on solving probe rf electronics problems and customer support. His current research interests include rf and magnetism modeling of NMR probes.

PART I REVIEW QUESTIONS

1. The CRC Handbook give the cgs molar susceptibility of NiO as 660E-6 and specific gravity as 6.67. What is its SI volumetric susceptibility?
2. A uniform, right, diamagnetic cylinder of length $6d$ is placed in a uniform external magnetic field $\mathbf{B}_0$. Which of the following statements is (are) correct?
   a. The field is uniform everywhere within the cylinder.
   b. The field is uniform within the cylinder except within $\sim 2d$ of the ends for any orientation.
   c. The field is uniform everywhere within the cylinder when aligned at the magic angle.
   d. The field is uniform along the axis for any orientation.
   e. The field is uniform along the axis when aligned at the magic angle.
3. A magic diamagnetic cylinder, length $0.56d$, is aligned with the uniform external magnetic field $\mathbf{B}_0$. Which of the following statements is (are) correct?
   a. The field is uniform along the axis.
   b. The field at the center is the same as for a sphere of equal susceptibility.
   c. The field may be shimmed to reasonable uniformity using only a very strong Z^2 shim.
   d. The field inside a spherical cavity at its center is exactly $\mathbf{B}_0$.
4. Using the method of effective surface currents and the field for the finite solenoid, calculate the relative B_0 shift inside a flat-bottomed cylinder of water 10 mm in diameter and 40 mm long, aligned with uniform B_0, on the axis, 10 mm from one end. Neglect the container.
5. Calculate the approximate relative B_0 shift in the sample from a macor air-fitting beneath the sample in a conventional HR liquids probe. Assume the fitting may be approximated as a cylinder of 12 mm OD, 5 mm ID, 50 mm length, coaxial with the sample, beginning 20 mm below the center of the sample. Use the method of dipole moments, then the method of effective surface currents. Why is there such a large discrepancy between the two answers? Which is correct?

6. NMR probe resolution is most likely to be limited by which type of magnetism in construction materials: (a) ferromagnetism, (b) paramagnetism, (c) diamagnetism?
7. Susceptibility matched plugs are *usually* used to
   a. Improve Q by reducing sample loading
   b. Improve S/N by allowing higher concentration with limited samples
   c. Reduce convection currents from thermal gradients
   d. Improve B_1 homogeneity throughout the sample
8. Place the following components or features in order, from most to least significant, with regards to degradation of resolution and lineshape in a conventional 5-mm HR, NB, liquids probe with an inner multi-X and an outer ^{1}H saddle coil.
   a. Standard brass screws in tuning capacitors 25 mm from the sample.
   b. An inner rf lead shield of 0.02-mm high-purity copper foil.
   c. A droplet of common epoxy, 0.6-mm sphere, in the center of the coil window.
   d. An inner coil of OFHC Cu foil, 0.04 mm thick.
   e. An accurately compensated inner coil of Cu-CuNi-Cu sandwich foil, 0.15 mm thick.
   f. An inner four-turn saddle coil of common no. 24 copper wire.
   g. An outer coil of OFHC Cu foil, 0.05 mm thick.
   h. A standard, nonmagnetic chip capacitor 6 mm below the window.
9. A magnetically compensated epoxy resin with improved rf power handling and thermal conductivity
   a. Is a pipe dream.
   b. Is likely to have narrow proton backgrounds.
   c. May contain finely powdered Si_3N_4 and Cr_2O_3.
   d. Probably contains silica and Teflon.
10. MAS at sufficiently high speeds completely averages
    a. All inhomogeneities.
    b. All field inhomogeneities of dipolar origin.
    c. All cylindrically symmetric inhomogeneities.
    d. All cylindrically symmetric isotropic dipolar inhomogeneities.